Towards the First Plasma-Electron Screening Experiment

Daniel Casey, Chris Weber, Alex Zylstra, Charlie Cerjan, Ed Hartouni, Matthias Hohenberger, Laurent Divol, Neel Kabadi, Brandon Lahmann, M. Gatu Johnson, J. Frenje

Abstract

The enhancement of fusion reaction rates in a thermonuclear plasma by electron screening of the Coulomb barrier is an important plasma-nuclear effect that is present in stellar models but has not been experimentally observed. Experiments using inertial confinement fusion (ICF) implosions may provide a unique opportunity to observe this important plasma-nuclear effect. Herein, we show experiments at the National Ignition Facility (NIF) have reached the relevant physical regime with respect to the density and temperature conditions but the estimated impacts of plasma screening on nuclear reaction rates are currently too low and need to be increased to make an observation within the expected measurement uncertainty. Detailed radiation hydrodynamics simulations show that practical target changes, like adding readily available high-Z gases, and significantly slowing the inflight implosion velocity while maintaining inflight kinetic energy, might be able to push these conditions to those where plasma screening effects may be measurable. We also perform synthetic data exercises to help understand where the anticipated experimental uncertainties will become important. But challenges remain such as detectability of the reaction products, non-thermal plasma effects, species separation, and impacts of spatial and temporal gradients. This work lays the foundation for future efforts to develop an important platform capable of the first plasma electron screening observation.

Introduction

For decades, numerous research groups have identified plasma-electron screening as an important physical process worth pursuing in high-energy-density (HED) experiments. For example, the National Research Council [1] describes a "raging debate" surrounding questions related to plasma screening models and that HED experiments may be well suited to help. In fact, ideas emerge periodically from the literature challenging the established models exacerbated by the complete lack of experimental data. This screening process becomes important as nuclei undergo a fusion reaction when their kinetic energy overcomes the repulsive Coulomb force and exploits favorable binding energy. In many HED environments where these reactions are occurring, such as in stellar cores or inertial confinement fusion implosions, the nuclei are embedded in a plasma. The background electrons in this plasma can lower the Coulomb barrier, enhancing their reactivity.

Plasma screening of nuclear reactions occurs when ions within the plasma interact with a Coulomb potential energy of $U(r) = \frac{Z_1 e^2}{r}$. Due to this potential, electrons will cluster around the ion and reduce the potential by a factor $U_{screen} = \frac{Z_1 e^2}{\lambda_D}$, where λ_D is the Debye length, $\lambda_D^2 = \frac{\varepsilon_0 \, k_B T}{n \, e^2}$. This results in an enhancement of the cross section of [2-4]

$$\frac{\sigma_{screened}(E)}{\sigma(E)} \approx \exp\left(Z_1 Z_2 \tilde{Z} \Lambda_0\right)$$
$$\approx \exp\left(\frac{Z_1 Z_2 e^2}{4\pi\epsilon_0 T \lambda_D}\right)$$

where Λ_0 is the charge-free plasma parameter, $(4\pi)^{\frac{1}{2}} e^3 n^{\frac{1}{2}}/(kT)^{3/2}$.

A similar screening effect occurs in accelerators that study nuclear reactions. In accelerator experiments, the bound electrons on the target screens the nucleus and enhances the reaction rate since the targets are not sufficiently hot to be plasmas. This effect, differing from plasma screening, must be removed to compute the bare nuclear cross section. This effect is significant for low center-of-mass energy cross sections and has in some cases been observed to be ~1.7-1.8x larger than expected [5] [6].

Despite widespread interest, the realization of a nuclear plasma screening experiment has been elusive because of several daunting challenges. First, extreme density and temperature conditions must be produced and diagnosed. Second, precise nuclear cross-section measurements must be made directly in the presence of strong density and temperature gradients. Finally, as the effect on fusion rates is often weak in the regimes that can be reproduced in the laboratory, care must be excised to develop a test where the magnitude of the measurement is expected to exceed the experimental uncertainties. The first two challenges were recently overcome using gas-filled indirect-drive experiments at the NIF [7]. Likewise, the 3He+T gamma cross-section was obtained [8] and the emitted 3He+T and 3He+3He reaction products have been recovered from ICF experiments at OMEGA [9]. This demonstrates the nuclear physics and cross-section experiments can be conducted in the complex environments of ICF implosions. We seek to partly address the third challenge by assessing whether these ICF implosions can produce conditions where this screening effect is expected to be large enough to be measured.

The generation of thermonuclear plasmas at the National Ignition Facility (NIF) may enable an initial observation of plasma screening of nuclear reactions. Inertial Confinement Fusion (ICF) experiments at NIF use 192 laser beams, totaling up to 1.9 MJ of energy, to irradiate the inside of a gold or uranium cylindrical enclosure (“hohlraum"). This creates an x-ray environment that ablatively implodes a spherical capsule. When the capsule compresses by 20-40x, the central hot-spot can reach temperatures of 2-6 keV and densities of 1-100 g/cm^3.

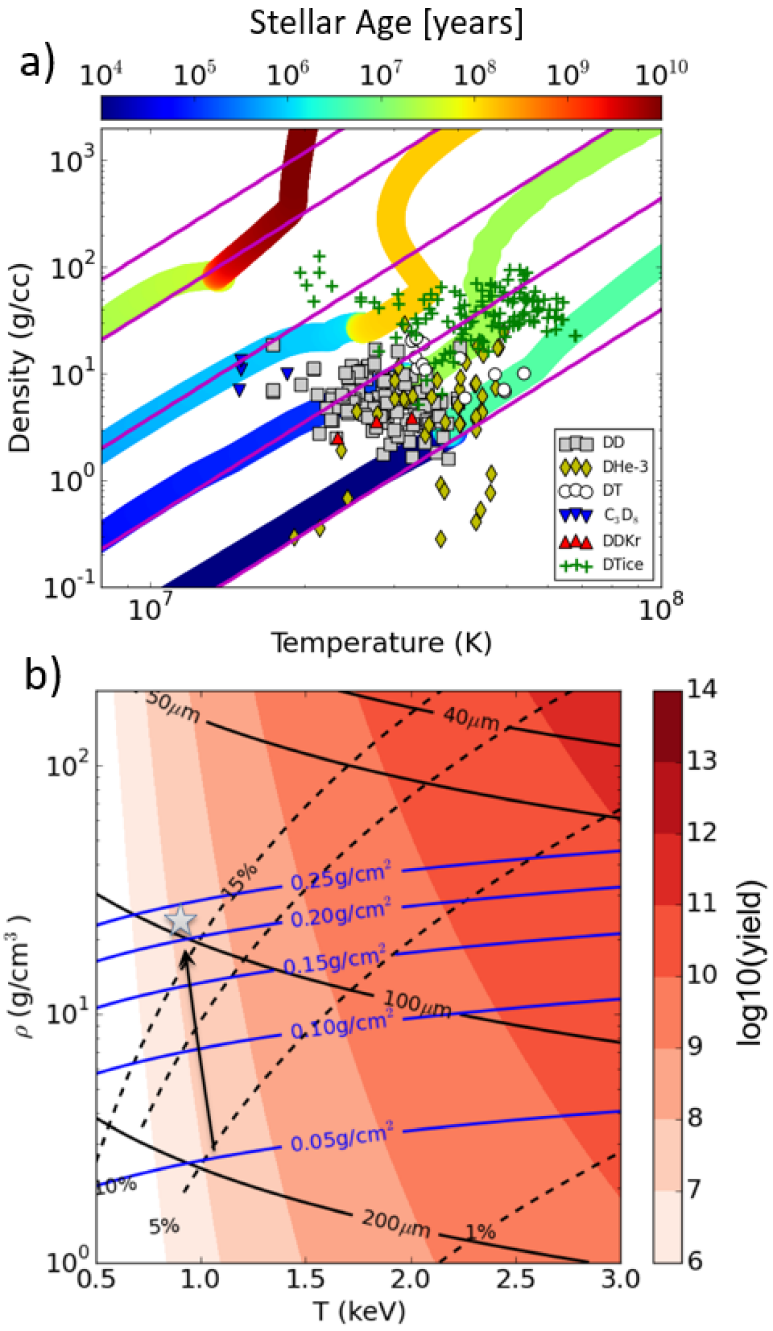

Figure 1 a) Stellar conditions compared with NIF experiments. b) Design space considering various requirements of a potential screening experiment.

Figure 1a shows inferences of density and temperature from various NIF implosions compared to the trajectories of relevant stars during the main hydrogen burning phase of their lifetime. The points plotted on top show that implosion conditions on NIF are very similar to that of stars during most of their lifetime. The green '+' symbols show implosion that have a cryogenic DT ice layer. The cryogenic layer allows the implosion to achieve higher compression reach larger densities. We are more interested in the other points, which are gas-filled capsules (symcaps) and provide more flexibility in the gas composition. In following sections we will detail the feasibility of D-^{3}He filled capsules, but a couple other cases stand out here. The red points show the effect of the addition of krypton gas (0.01, 0.02 and 0.03 atomic percent), which cools the implosion temperature. A similar effect is seen in the C3D8 (deuterated propane) implosions, which have cooler temperatures than the other cases. This effect pushes the screening enhancement up to 3%.

A measurement with increased screening requires that: 1) the screening enhancement is larger than measurement uncertainty, 2) the total yield is at a measurable level, and, 3) if measuring escaping protons, the areal density must be low enough that they will escape and reach the detector. To find conditions in density-temperature space where a good screening measurement will occur, consider an inertially confined sphere of plasma with a density ρ, temperature T, and radius R. This sphere will disassemble in a time $t \sim R/c_s$, where c_s is the speed of sound. Using this disassembly time as the burn duration, we can estimate the yield, ρR, and screening enhancement, shown in Figure

1b. The screening enhancment increases as one travels vertically along a contour of constant yield. For a measureable proton signature, the ρR must be kept below ~0.2-0.25g/cm^2. For a yield of 10^7, this limits the maximum screening amount to ~15% enhancement. Increasing the number of plasma electrons by adding a high Z dopant to the gas can also increase the screening at a given density and temperature.

To observe the impact of screening, we propose to observe the relative ratio of fusion products from D^{3}He (protons or gammas) and DD (neutrons) reactions emitted in the same ICF implosion. Then, following the same procedure developed in [7] and [10], we plan to use this to infer the relative reactivities (R is the D^{3}He/DD reactivity ratio $R = \langle\sigma v\rangle_{12}/\langle\sigma v\rangle_{11}$) in the presence of plasma-electron screening. The procedure developed in [7] should be modified with the inclusion of an additional term for very low temperatures where a screening measurement would likely operate. This term brings in the effect of temporal and spatial gradients because of the temperature dependence of R in the range of interest, unlike the DT/DD reactivity in the prior study. The result is: $\frac{Y_{\mathrm{DD}}}{Y_{\mathrm{D3He}}} = \frac{1}{2}\frac{f_D}{f_{3\mathrm{He}}} R_0 \left[1 + \frac{1}{R_0}\ \frac{\partial R}{\partial T}\left[\langle T_{\mathrm{D3He}}\rangle - \langle T_{\mathrm{DD}}\rangle\right]\right]$,

and that $\langle T_{\mathrm{D3He}}\rangle - \langle T_{\mathrm{DD}}\rangle = \frac{1}{2}\left[\frac{1}{R_0}\ \frac{\partial R}{\partial T}\right]^{-1}\left[1 - \sqrt{1 - \left(2\frac{1}{R_0}\ \frac{\partial R}{\partial T}\sigma_{T-\mathrm{D3He}}\right)^2}\right]$,

where σ_T is the width of the burning temperature distribution, and the terms R_0 and $\frac{\partial R}{\partial T}$ are evaluated at $\langle T_{\mathrm{DD}}\rangle$. The second equation may become important as $\langle T_{\mathrm{D3He}}\rangle$ may prove difficult to directly measure but $\langle T_{\mathrm{D3He}}\rangle - \langle T_{\mathrm{DD}}\rangle$ could be inferred if $\sigma_{T-\mathrm{D3He}}$ can be determined from moments of the DD neutron spectrum [11] or estimated from models of the platform.

If the S-factor is non-resonant within the region of the reacting nuclei, the term $\frac{1}{R_0}\ \frac{\partial R}{\partial T}$ can be estimated simply assuming barrier penetrability and geometric factors dominate the energy dependance over the burn. The result is: $\frac{1}{R_0}\ \frac{\partial R}{\partial T} = \frac{K}{9}\ \left[\frac{4}{T^{7/3}} + \frac{K}{T^{8/3}}\right]$, where $K = \frac{-3\left(\pi\,\alpha_f\right)^{2/3}\left(m_p c^2\right)^{1/3}}{2^{1/3}}\left[\left(\frac{{Z_1}^4\,A_1}{2}\right)^{1/3} - \left(\frac{(Z_1 Z_2)^2\,A_1 A_2}{A_1 + A_2}\right)^{1/3}\right]$. Here, 1 and 2 is for each reactant, Ts are the temperatures, Zs are the atomic numbers, As are the atomics masses, α_f is the fine structure constant, $m_p c^2$ is the rest mass energy of the proton. and This is especially useful, because it allow us to make estimates of how the relative energy dependance of the cross-sections might weight with the reacting ion distributions without needing to know the absolute cross-sections themselves. $\frac{1}{R_0}\ \frac{\partial R}{\partial T}$ is shown the region of interest in Figure 2 below.

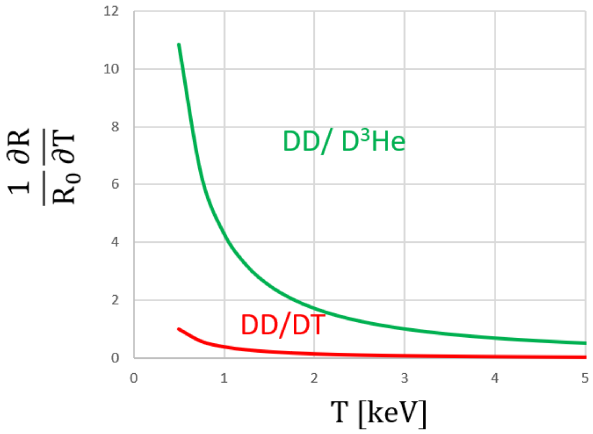

Figure 2 – Plot of the temperature dependance of the relative reactant reactivities ($R = \langle\sigma v\rangle_{12}/\langle\sigma v\rangle_{11}$) for DD and D3He.

To evaluate how spatial and temporal profiles impact burn weighted quantities like yield and temperature, a simple hotspot model developed Betti [12] can be used. Figure 3 shows the results of reactant distribution in space at peak compression (a and c) and evolutions in time (b and d) for two example implosions. The yields and temperatures are shown in the tables to the right. This sort of synthetic data exercise can enable tests of the equation presented earlier and provide at least some indication on whether the presence of temperature and density gradients are an issue.

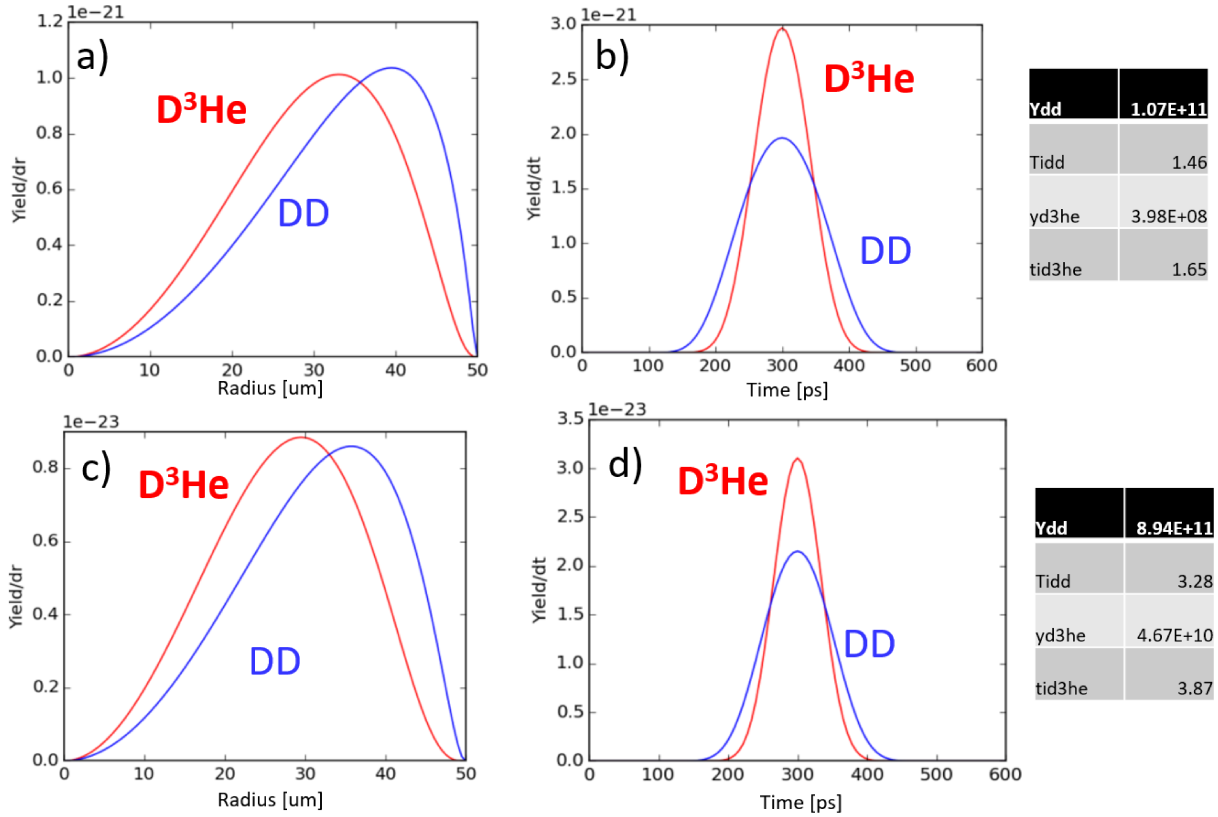

Ydd	1.07E+11
Tidd	1.46
yd3he	3.98E+08
tid3he	1.65

Ydd	8.94E+11
Tidd	3.28
yd3he	4.67E+10
tid3he	3.87

Figure 3 – DD and D3He reactant distribution in space and time using a numeric hotspot model to estimate the impact of temporal and spatial gradients on burn-weighted quantities for two different example implosions.

Figure 4a shows the results of comparing the analytic equation for $\langle T_{\mathrm{D3He}} \rangle - \langle T_{\mathrm{DD}} \rangle$ vs the numeric calculation with the hotspot model. The results show at 5 different representative temperatures that the analytic equation works very well is reactant distribution width $\sigma_{T-\mathrm{D3He}}$ is known, a key point to consider. Figure 4b shows the results of comparing $\langle T_{\mathrm{DT}} \rangle - \langle T_{\mathrm{DD}} \rangle$ vs actual experimental data from a variety of implosion platforms. Here, the $\sigma_{T-\mathrm{DT}}$ was calculated from two representative 1D radiation hydrodynamic simulations using the code HYDRA [13] for a indirect drive exploding pusher [14] and a DT filled symcap [15]. The curve with predicted $\sigma_{T-\mathrm{DT}}$ appears to significant under predict the data, an observation in line with those of Gatu-Johnson[16]. However, if $\sigma_{T-\mathrm{DT}}$ is increased by 1.6x then a good match to the measured trend is reproduced. It is unclear the exact reasons for this but it could be the enhancement of $\sigma_{T-\mathrm{DT}}$ due to 2 and 3D effects not well captured by the 1D HYDRA simulations. This fact may motivate specific experiments to determine $\sigma_{T-\mathrm{DT}}$ in a future plasma screening experiment. For example, adding trace tritium in a principle D^3He may allow the measurement of the $\langle T_{\mathrm{DT}} \rangle$and$\langle T_{\mathrm{DD}} \rangle$ in a three component plasma providing some constraint on the third unmeasured $\langle T_{\mathrm{D3He}} \rangle$.

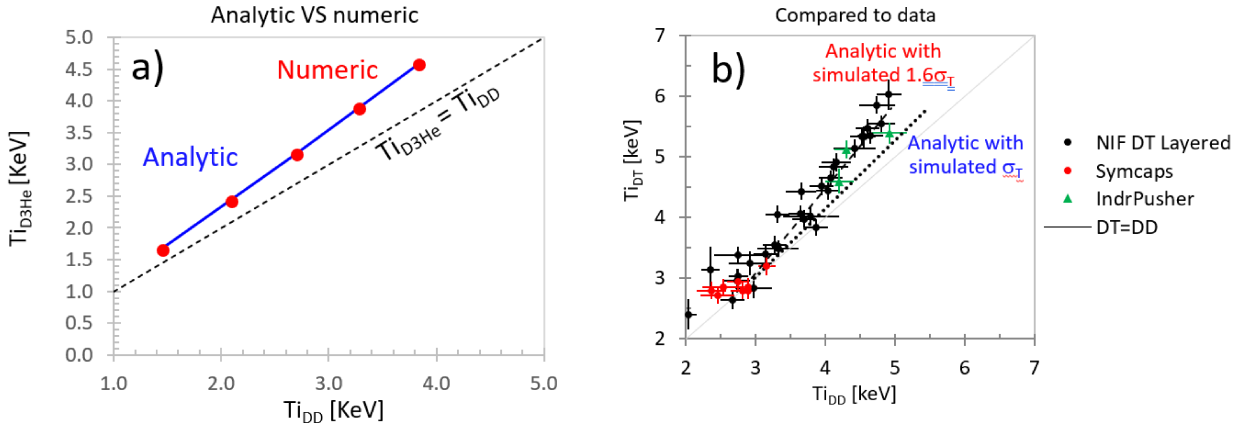

Figure 4 - a) Comparison of $\langle T_{D3He} \rangle - \langle T_{DD} \rangle$ estimated using the analytic calculation of vs numeric integration assuming a Betti 1D hotspot profile [12]. Comparison of the analytic $\langle T_{DT} \rangle - \langle T_{DD} \rangle$ assuming σ_T simulated by hydra vs measured data and analytic curve with σ_T increased by 1.6x.

As a check on how the formula for how to extract the reactivity ratio will work with these predicted gradients, the ENDF evaluated cross sections were input [17] with the 1d Betti hotspot profile from which the yields and temperatures were calculated and used to attempt to recover the reactivity input in the calculation. The results are shown in Figure 5 and indicate that in the presence of this level of temperature variation, the extracted reactivity ratio is recovered.

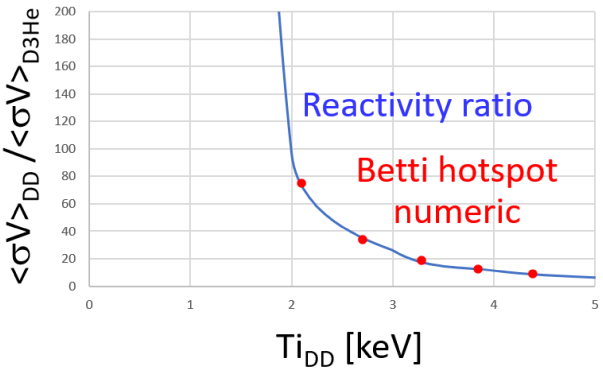

Figure 5 – Comparison of the reaction ratio for DD and D3He vs the extracted reactivity ratio using a synthetic data set calculated using a Betti 1D hotspot profile [12].

To attempt to observe screening in an ICF experiment, two principal design paths are being actively explored . The first would use as the primary measurement D^3He protons that require the total areal density not exceed the ~15 MeV proton range and detected with WRF or step range filters [18] placed near the implosion. Existing data in gas filled implosions was examined to assess the ability to measure D^3He protons from implosions with moderately high compression areal density and from which to determine the reactivity $<\sigma v>_{D3He}$ in density and temperature conditions where screening is expected to be weak. This work initially encountered significant detector analysis challenges with low energy protons (~7 MeV) which were resolved [19]. [Anything more we should say about ongoing DS exps?]

An alternative design path is to maximize yield at high hotspot density for measurements of the D^3He gamma ray (branching ratio ~ 1e-4) [20], since gammas and neutrons can escape high areal density implosions. This measurement would require a high solid angle Cherenkov detector [ref?]. Since these detectors have high systematic uncertainties, we would measure the D^3He/DD yield ratio at both screening-relevant conditions and in a low-density plasma (exploding pusher) to eliminate systematics. HYDRA simulations explored the potential parameter space and have found several interesting designs that look promising in each of these design directions. The results in Figure 2 shows that estimated screening corrections greater than 10% can be achieved, but most of these simulated designs would be significantly challenging to measure. Of these, some designs show some potential (marked as black-outlined points), where the areal density is low enough to allow the protons to escape (circles) or the yield is high enough to allow a gamma measurement (diamonds).

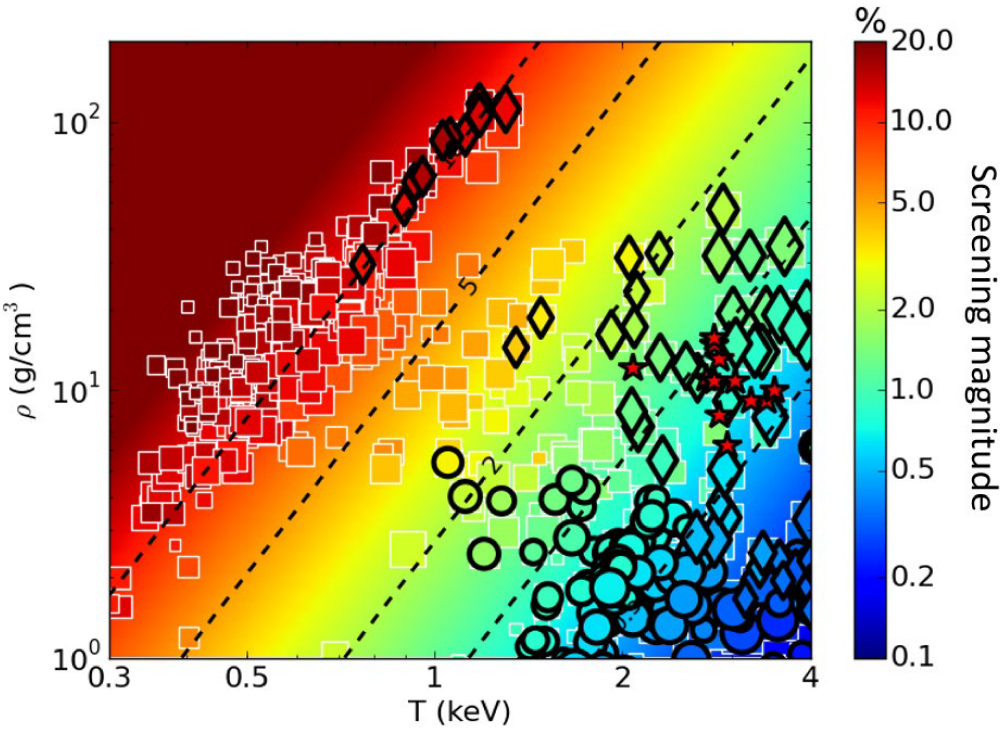

Figure 6 Ensemble of HYDRA simulations of capsule implosions. Several designs show significant screening and the most promising are outlined in black

One particular HYDRA simulated example point in Figure 3 is explored in more detail in Figure 4. This design uses a large capsule, 1400 microns inner radius and 200 microns thick. The large capsule ensures that high areal density will remain to produce a prominent compression phase. Figure 4b shows that after the shock flash, the Kr mixed in with the gas cools the hot spot and it reaches an iso-thermal state near 1keV lasting for almost 1ns. For perspective, typical NIF implosions are confined for almost an order of magnitude less time than this. This interesting set of implosion dynamics is established because the temperature and density conditions allow it to enter a radiation dominated energy loss regime, rather than the more typical thermal conduction dominated regimes of most hotspot ICF designs. This radiation dominated isothermal system is interesting enough to warrant study just to understand this radiation dominated physics regime but importantly also produces conditions where screening becomes non-negligible, as shown in the subplot of the reaction rate and time dependent screening magnitude Figure 4.

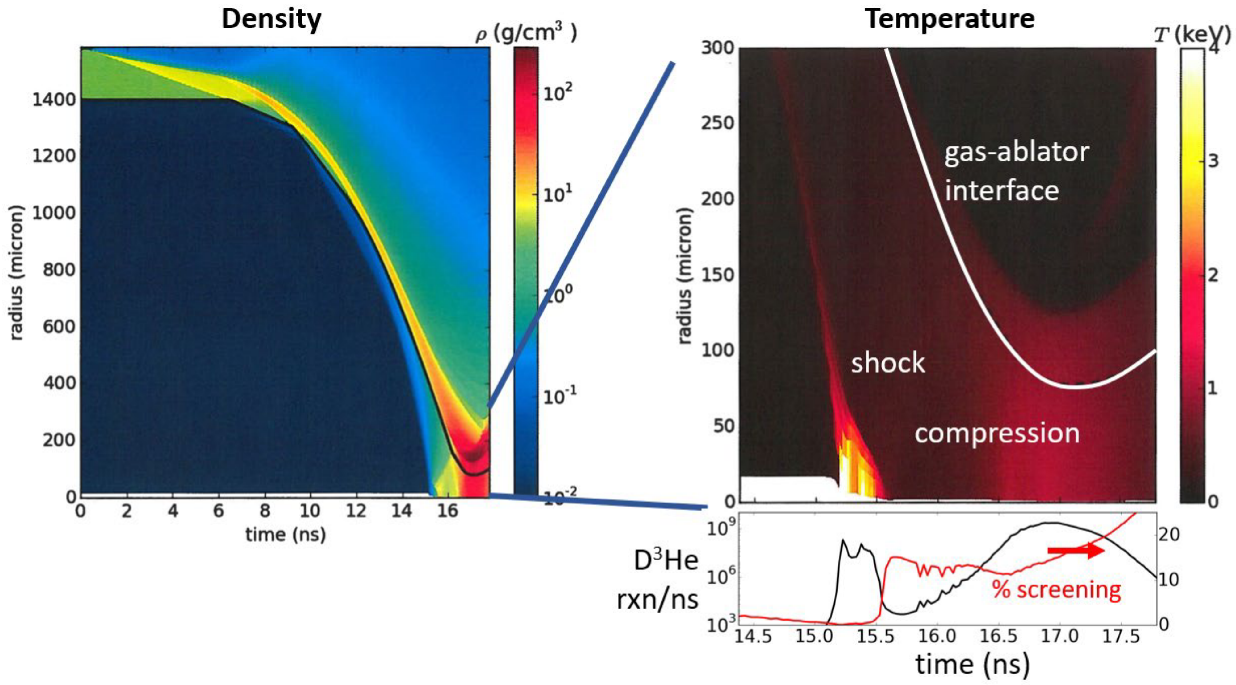

Figure 7 - a) HYDRA simulation of radius vs time for an example screening experiment design candidate. The hotspot density reaches high conditions ~100 g/cc. b) Zoom in temperature dynamics showing a brief shock flash and extended compression phase. Also shown are the reaction rate and screening magnitude of this design.

The design space of interest for observing screening is expected to produce neutron yields from DD fusion of order 10^7 to 10^8 neutrons. This also presents a challenge to the neutron time-of-flight spectrometry that will be used to measure the yield and ion temperature of the implosions. The current analysis process [21] was modified to include neutron elastic scattering from both the D^3He and the ablator shell.

This analysis was then performed on shot data, in particular N160410-001, and on the Hydra post-shot neutron spectrum. The post-shot spectrum was transformed into synthetic neutron time-of-flight including the various features of the neutron transport, detection and digitization. This time-of-flight data was then analyzed and compared to the shot data. Figure 4 shows the results of this process.

This analysis tool will allow the simulation generated neutron spectra to be generated and analyzed to investigate the of statistical significance of both yield and ion temperature.

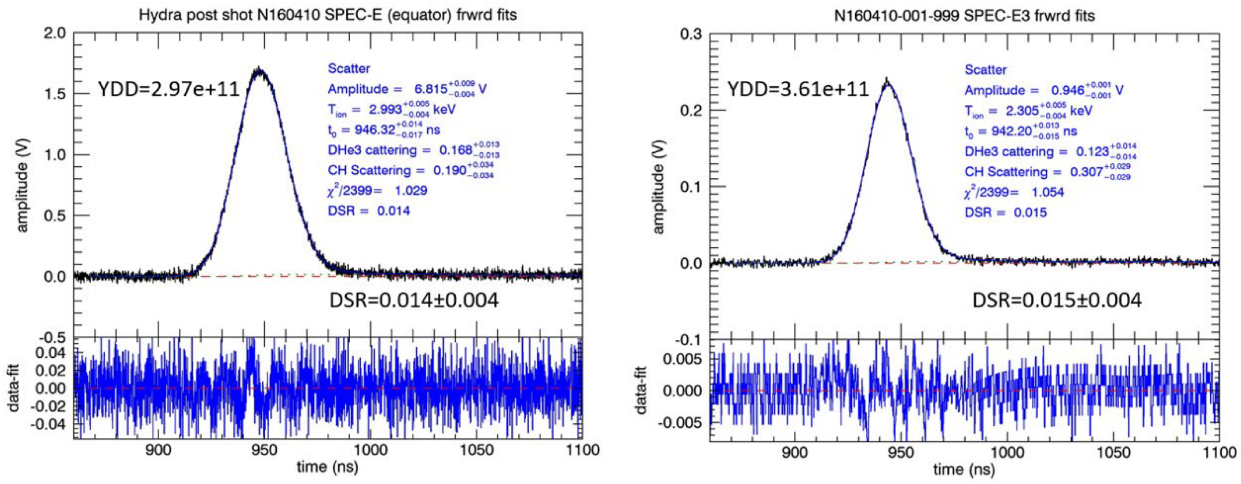

Figure 8 - The result of a forward fit model to, a.) the data from shot N160410-001 and b.) of the synthetic neutron time-of-flight spectrum generated in post-shot Hydra simulation. Included in the forward fit model are the effects of neutron scattering from the CH ablator shell and the compressed D^3He fuel. The "down scatter ratio," DSR, is fraction of yield for neutrons of energy 1.9 to 2.2 MeV divided by the yield from 2.2 to 2.7 MeV

This initial work assessed the issues with respect to a plasma screening measurement and identified some credible solutions to long standing challenges. The next step is to test then null hypothesis of implosions where screening is expected to be negligible. Then the physics of the radiation dominated implosion should explored and tested to see if indeed the required conditions are achieved, and assess of the reaction products will be measurable. While substantial challenges remain, we have shown that experiments on NIF show promise and may enable the first observation of plasma screening of nuclear reactions, addressing one of the fundamental questions of high-energy-density physics.

References

[1] R. C. Davidson et al., *National Research Council: Frontiers in High Energy Density Physics: The X-Games of Contemporary Science* (The National Academies Press, Washington, DC, 2003).

[2] J. N. Bahcall, L. S. Brown, A. Gruzinov, and R. F. Sawyer, A&A **383**, 291 (2002).

[3] H. Dzitko, S. Turck-Chieze, P. Delbourgo-Salvador, and C. Lagrange, Astrophysical Journal **447**, 428 (1995).

[4] E. Salpeter, Australian Journal of Physics **7**, 373 (1954).

[5] M. Aliotta *et al.*, Nuclear Physics A **690**, 790 (2001).

[6] U. Schröder, S. Engstler, A. Krauss, K. Neldner, C. Rolfs, E. Somorjai, and K. Langanke, Nuclear Instruments and Methods in Physics Research Section B: Beam Interactions with Materials and Atoms **40-41**, 466 (1989).

[7] D. T. Casey *et al.*, Nature Physics **13**, 1227 (2017).

[8] A. B. Zylstra *et al.*, Physical Review Letters **117**, 035002 (2016).

[9] A. B. Zylstra *et al.*, Physical Review Letters **119**, 222701 (2017).

[10] N. V. Kabadi *et al.*, Physics of Plasmas **28**, 022701 (2021).

[11] D. H. Munro, Nuclear Fusion **56**, 036001 (2016).
[12] R. Betti, M. Umansky, V. Lobatchev, V. N. Goncharov, and R. L. McCrory, *Hot-spot dynamics and deceleration-phase Rayleigh?Taylor instability of imploding inertial confinement fusion capsules* (AIP, 2001), Vol. 8, 12.
[13] M. M. Marinak, G. D. Kerbel, N. A. Gentile, O. Jones, D. Munro, S. Pollaine, T. R. Dittrich, and S. W. Haan, Physics of Plasmas **8**, 2275 (2001).
[14] S. Le Pape *et al.*, Physical Review Letters **112**, 225002 (2014).
[15] D. J. Schlossberg *et al.*, Physical Review Letters **127**, 125001 (2021).
[16] M. Gatu Johnson *et al.*, Physical Review E **94**, 021202 (2016).
[17] M. B. Chadwick *et al.*, Nuclear Data Sheets **107**, 2931 (2006).
[18] F. H. Seguin *et al.*, Review of Scientific Instruments **74**, 975 (2003).
[19] N. Kabadi, Ph.D. dissertation, MIT, 2022
[20] Y. Kim *et al.*, Physics of Plasmas **19**, 056313 (2012).
[21] R. Hatarik *et al.*, Journal of Applied Physics **118**, 184502 (2015).